Superconducting condensate residing on small Fermi pockets in underdoped cuprates

V. M. Krasnov*

Department of Physics, Stockholm University, AlbaNova University Center, SE-10691 Stockholm, Sweden

(Received 28 November 2014; revised manuscript received 8 May 2015; published 16 June 2015)

How does Fermi surface develop upon doping of cuprates, does it consist of large barrels or small pockets, which of them is responsible for superconductivity, and what is a role of the pseudogap? Those are actively debated questions, important for understanding of high temperature superconductivity. We study doping dependence of intrinsic tunneling in $Bi_2Sr_2Ca_{1-x}Y_xCu_2O_{8+\delta}$ cuprates, which allows independent analysis of Cooper pair and quasiparticle transport. We observe that with decreasing doping the supercurrent is rapidly decreasing at a rate much faster than the doping level, but the quasiparticle resistance at a sufficiently high bias remains almost doping independent. This remarkable discrepancy indicates that Cooper pairs and quasiparticles are originating from different parts of the Brillouin zone: Cooper pairs are residing on small pockets, which are progressively shrinking with decreasing doping, but the majority of the quasiparticle current is integrated over large barrels, which are only weakly doping dependent. The expanding pseudogap areas along the barrels do not contribute to pair current. This provides direct evidence for nonsuperconducting origin of the pseudogap. We present numerical calculations, taking into account Fermi surface topology, that support our conclusions.

DOI: 10.1103/PhysRevB.91.224508 PACS number(s): 74.72.Kf, 74.25.Jb, 74.50.+r, 74.78.Fk

I. INTRODUCTION

Fermi surface in metals occurs at an intersection of a conduction band with a chemical potential. Insulators do not have Fermi surface because the chemical potential lies in the band gap region. High temperature superconductivity in cuprates appears upon doping of a Mott insulator. How does Fermi surface develop with doping [1,2], does it consist of large barrels or small pockets, which of them is responsible for superconductivity, and what is a role of the pseudogap that affects the topology of Fermi surface? Those are actively debated questions, important for the understanding of high temperature superconductivity.

According to Luttinger theorem, for a two-dimensional doped insulator a relative area of the Fermi surface with respect to the Brillouin zone should be equal to the number of charge carriers in the unit cell (per spin) irrespective of the strength of electronic correlations. Therefore, Fermi surface area in cuprates should be proportional to doping p. However, a photoemission edge in cuprates forms large barrels with an area $\propto 1+p$, corresponding to a half-filled Brillouin zone, already at low doping [2–4]. This may indicate a violation of Luttinger theorem [5], or a need for a more careful interpretation of data. Indeed, strictly speaking, only nodal parts of the barrels (Fermi arcs) [4,6] are representing the true Fermi surface because antinodal parts are affected by the pseudogap (PG) [7–15]. Luttinger theorem can be satisfied assuming that arcs represent small Fermi pockets [4,16–21]. Although existence of such pockets was confirmed by quantum oscillation experiments [22–27], their position [1], connection to barrels, and significance for superconductivity remains unclear [28].

Answers to questions posted above depend essentially on interpretation of the PG. If the PG represents a precursor of the superconducting gap (SG) Δ_{SG} [13,29] then antinodal parts of barrels should contain the major part of the superconducting condensate. On the other hand, there are indications of nonsuperconducting origin of the PG [8–10,18,28,30–34]. Such PG may represent either a residual insulator gap [4,33], or some coexisting hidden order like spin/orbital/charge density wave [28,34], which competes with superconductivity. In this case PG parts of barrels should not contain the superconducting condensate, which should instead reside only on PG-free nodal arcs/pockets. A possibility of coexistence of precursor superconductivity and competing PG at $T > T_c$ was also discussed [35,36]. Discrimination between SG and PG is particularly difficult at $T < T_c$, when the whole barrel (except nodal points) is gapped. So far it is not possible to conclude whether superconductivity is originating from large barrels or small Fermi pockets.

Here we study doping dependence of current-voltage (I-V) characteristics of intrinsic Josephson junctions in $Bi_2Sr_2Ca_{1-x}Y_xCu_2O_{8+\delta}$ (Bi-2212) cuprate. We utilize their ability to independently probe Cooper pair and quasiparticle (QP) currents. It is observed that with decreasing doping the supercurrent is rapidly decreasing at a rate much faster than p, but the QP resistance remains almost unchanged. This indicates that pairs and QPs originate from different parts of the Brillouin zone: The QP current is integrated over the full length of large barrels, which are only weakly doping dependent, but Cooper pairs are residing on small pockets, which are progressively shrinking with decreasing doping. Antinodal PG parts of barrels, which grow with underdoping, do not contribute to supercurrent. This provides direct evidence for nonsuperconducting origin of the PG. We present numerical calculations, taking into account Fermi surface topology, that support our conclusions.

The paper is organized as follows. In Sec. II we describe details of intrinsic tunneling experiments, show current-voltage I-V characteristics at different doping, and clarify extraction of parameters. In Sec. III we present results of numerical modeling of interlayer I-V characteristics taking into consideration Fermi surface topology and material parameters of Bi-2212. In Sec. IV we perform detailed analysis of obtained doping dependencies of intrinsic tunneling characteristics, calculate

*vladimir.krasnov@fysik.su.se

dependence of the critical current on the arc/pocket size, and discuss model independence of conclusions.

II. INTRINSIC TUNNELING SPECTROSCOPY

Intrinsic Josephson junctions are naturally formed in Bi-2212 single crystals [37]. Superconducting electrodes are formed by CuO_2-Ca-CuO_2 and the tunnel barrier by SrO-2BiO-SrO atomic layers. Intrinsic tunneling has several advantages, compared to other spectroscopic techniques. First of all, it probes *bulk* electronic properties, not sensitive to surface effects [30]. Another important advantage, which we utilize in this work, is its ability to independently probe both Copper pair and QP transport. This is brought about by a large quality factor $Q = \sqrt{2\pi c I_c C R_n^2/\Phi_0}$ of such SIS (superconductor-insulator-superconductor) type junctions. Here c is the speed of light in vacuum, I_c is the Josephson critical current, C is the junction capacitance, R_n is the QP resistance, and Φ_0 is the flux quantum. The large $Q \sim 100$ of intrinsic Josephson junctions is caused by a large specific capacitance $C \sim 70$ fF/μm^2 [38] due to atomic separation between S electrodes and a large dielectric constant of a parent polar insulator. The I-V of a SIS junction exhibits a hysteresis with two separate branches. The zero-voltage branch corresponds to Cooper pair tunneling and the resistive branch to QP tunneling. The latter occurs because Josephson current at a finite voltage oscillates sinusoidally in time when $Q \gg 1$. Thus, it averages out to zero and does not contribute to direct current (see, e.g., Ref. [39]). The resistive part of the I-V in this case is caused solely by the QP tunneling. It depends on the QP density of states (DoS) creating the basis for the intrinsic tunneling spectroscopy technique. This peculiar separation of Cooper pair and QP contribution allows independent analysis of pair and single electron transport from intrinsic tunneling characteristics without any modeling.

Small mesa structures containing $N = 7$–12 junctions were made on top of freshly cleaved single crystals using micro/nanofabrication techniques. Details of sample fabrication and characterization can be found in Refs. [8,30,31,40]. Measurements are done in a ^{4}He cryostat at zero (ambient) magnetic field. The doping level was changed by annealing of crystals from the same batch at $T = 600\,^\circ$C and was estimated using an empirical expression $T_c(p) = T_c(\mathrm{OP})[1 - 82.6(p - 0.16)^2]$ [9], where $T_c(\mathrm{OP}) \simeq 95$ K is the maximum T_c at optimal doping (OP). An onset of superconductivity occurs at the insulator-to-metal transition at $p = 0.05$ and the optimal doping corresponds to $p = 0.16$ holes per Cu atom.

Figures 1(a) and 1(b) show temperature dependencies of I-V and dI/dV curves for a moderately underdoped (UD) mesa $p \simeq 0.14$ with an area 2×1.5 μm^2, containing $N = 10$ junctions. It is seen that I-V curves of such junctions exhibit a hysteresis with zero voltage and resistive branches

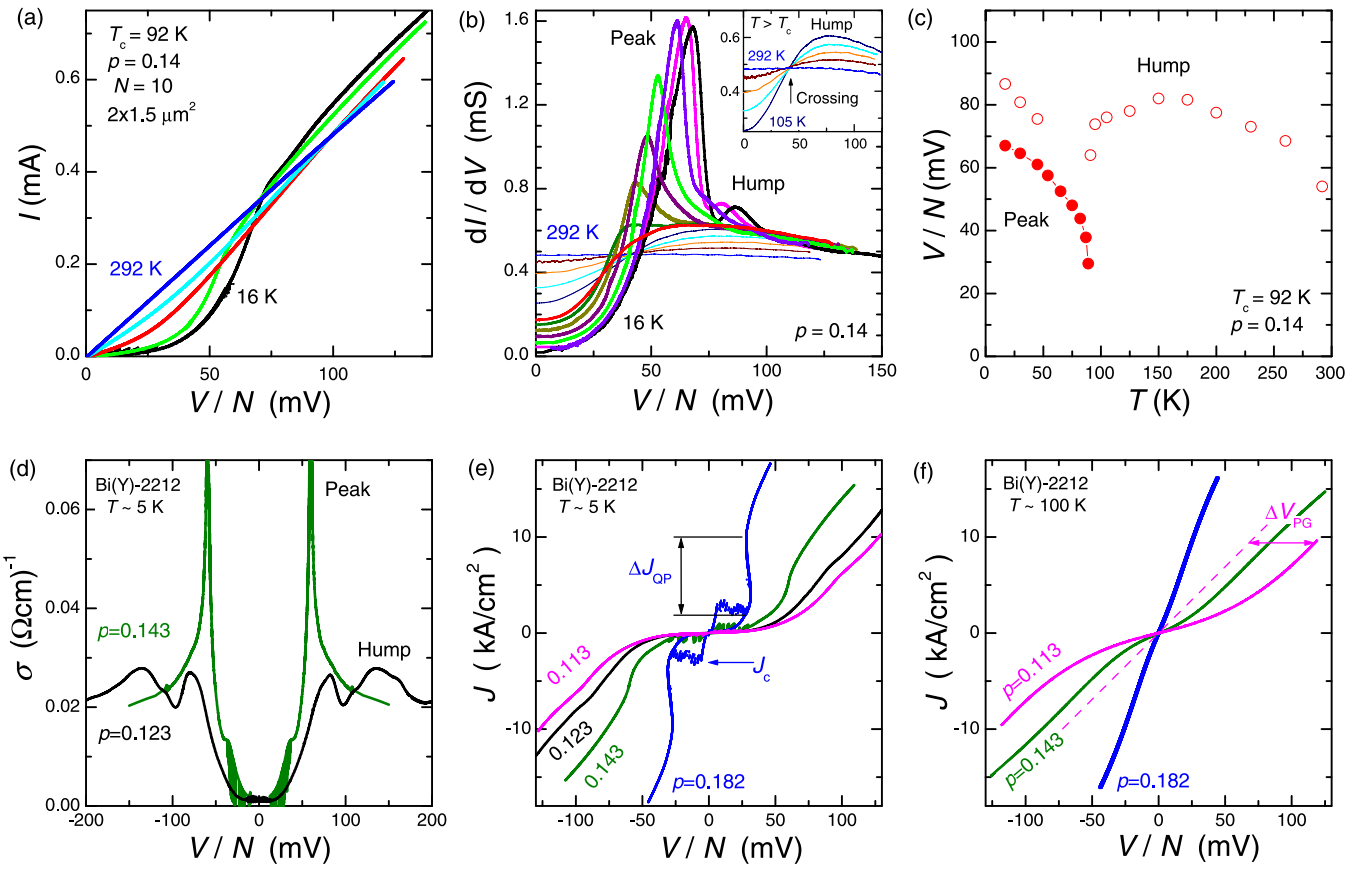

FIG. 1. (Color online) (a)–(c) Temperature dependencies of (a) I-V, (b) $dI/dV(V)$, and (c) the superconducting peak and the PG hump voltages for a moderately underdoped mesa $p = 0.14$. Inset in (b) demonstrates crossing of $dI/dV(V)$ curves at $T > T_c$ as a result of state-conserving filling of the PG. (d) Comparison of normalized intrinsic spectra for slightly and strongly underdoped mesas. (e) and (f) Comparison of normalized I-V curves at different doping in superconducting and normal states.

corresponding to a Cooper pair and QP tunneling, respectively [8,30,31,40–44]. This allows independent analysis of a bulk pair and QP transport inside the crystal.

At $T < T_c$ a sum-gap peak in dI/dV is seen at $V = 2\Delta_{SG}/e$ (per junction) followed by an almost T-independent tunnel resistance R_n. At $T > T_c$ the peak vanishes and only a broad PG hump remains visible. The peak and the hump exhibit autonomous behavior as a function of doping [10], temperature [8,30], and magnetic field [31]. With increasing T the hump is deflated in a state conserving manner leading to crossing of dI/dV curves [30,31,40], as demonstrated in the inset to Fig. 1(b).

Figure 1(c) shows T dependencies of superconducting peak and pseudogap hump voltages. It is seen that the peak vanishes in a mean-field manner upon approaching T_c [30]. The PG hump persists both below and above T_c. At $T < T_c$ the hump voltage is shifting together with the superconducting peak, indicating that the PG is affected by superconductivity so that the two gaps form a combined gap [30]. At $T > T_c$ the hump weakly depends on temperature. As seen from Fig. 1(b), upon approaching room temperature the hump rapidly looses its intensity (in a thermal-activation manner [30,40]) and eventually moves to lower voltage [10].

Figure 1(d) shows differential conductivity $\sigma = sN/AdI/dV$ curves for UD mesas with $p = 0.143$ and 0.123. Here A is the mesa area and $s = 1.55$ nm is the interlayer distance. For a strongly UD case $p = 0.123$ the peak is small and the hump is large. The hump coexists with the peak at $T \ll T_c$ [8,10] and has even larger amplitude than the peak. With increasing p the peak is growing and the hump is decreasing both in height and voltage. Close to optimal doping $p = 0.143$ the hump is buried under the peak. However, it is uncovered at elevated T as the peak shifts to lower voltages [8], as seen from Fig. 1(b). Figures 1(e) and 1(f) represent current density J vs voltage per junction for different p. Figure 1(e) represents data at low T and Fig. 1(f) above T_c. To facilitate direct comparison we normalized current and voltage scales by the mesa area and the number of junctions, respectively. The following main features, which will be in focus of our discussion.

(i) *The critical current.* Multiple branches appear due to one-by-one switching of junctions from the superconducting to the resistive state [8,37]. The amplitude of branches represents the critical current density J_c.

(ii) *The sum-gap kink amplitude.* ΔJ_{QP} represents a number of QPs within the SG, which are subjected to pairing. Therefore, ΔJ_{QP} and J_c should be connected. Indeed, both rapidly decrease with decreasing p.

(iii) *The pseudogap.* The I-V of the strongly UD mesa $p = 0.113$ is nonlinear at $T > T_c$. The current is suppressed below a threshold voltage ΔV_{PG}. ΔV_{PG} decreases with increasing p. For the overdoped (OD) mesa $p = 0.182$ the threshold disappears and the I-V becomes almost Ohmic.

(iv) *The tunnel resistance.* From Fig. 1(e) it is seen that the high-bias R_n is initially increasing with decreasing p, but for UD mesas the differential resistance becomes almost doping independent. Observation of a qualitative difference in doping dependencies of the supercurrent and the high-bias QP transport is the main new result, which will be in focus of our discussion.

Extraction of the critical current and the sum-gap kink amplitude is clarified in Fig. 2. Figures 2(a)–2(c) show current density versus voltage characteristics at low T (a) for an overdoped $p = 0.182$, (b) moderately underdoped $p = 0.143$, and (c) strongly underdoped $p = 0.113$ mesas. Multiple branches due to one-by-one switching of intrinsic Josephson junctions from the superconducting to the resistive state are clearly seen. Counting of the branches yield the number of junctions in the mesa. The critical current density J_c is estimated from the maximum amplitude of the branches, as shown by an arrow in Fig. 2(b).

Figures 2(d)–2(f) represent the differential conductivity versus current density plots for the same mesas. Corresponding I-Vs are shown in Fig. 1(e). The sum-gap kink amplitude ΔJ_{QP} is obtained from the width at the half-maximum of the sum-gap peak. The peak height is measured from the high bias conductivity level. Estimation of ΔJ_{QP} for all three mesas is marked by arrows in Figs. 2(d)–2(f).

III. MODELING OF INTERLAYER TUNNELING CHARACTERISTICS

To gain a better understanding of experimental data we performed numerical calculations taking into account the Fermi surface topology. Calculation of interlayer tunneling characteristics requires integration of QP current over all initial and final states, taking into account QP DoS, the band structure [45], angular dependence of the energy gap $\Delta(\varphi)$, and the transmission probability $\mathrm{Tr}(\varphi_1,\varphi_2)$ [46]. We describe initial and final states by momentum angles $\varphi_{1,2}$, with respect to the principle axis of the Brillouin zone. In the absence of the PG, analysis of various tunneling scenarios for coherent $\varphi_1 = \varphi_2$ and incoherent $\varphi_1 \neq \varphi_2$ tunneling between d-wave superconductors can be found in the Supplemental Material to Ref. [40] and in Ref. [47]. Here we will focus on analysis of the pseudogap effect for the case of coherent $\varphi_1 = \varphi_2$ and elastic (momentum and energy conserving) tunneling for a model of a "remnant" Fermi barrel with a PG in antinodal and a Fermi arc in the nodal parts. We assume that the arcs represent one side of small Fermi pockets, as shown in Fig. 3(a), and that Cooper pair tunneling occurs only in the Fermi-arc regions, while QP tunneling occurs along the whole length of barrels. All the characteristics are presented for a quarter of the Brillouin zone, sketched in Fig. 3(a), and are symmetrically reflected for other three quarters of the zone.

The QP tunneling current can be written as

$$I = A\int_0^{2\pi}\frac{d\varphi_1}{2\pi}\int_0^{2\pi}\frac{d\varphi_2}{2\pi}\int_{-\infty}^{+\infty}dE \times \mathrm{Tr}^2(\varphi_1,\varphi_2)N(E,\varphi_1)N(E+eV,\varphi_2) \times [f(E)-f(E+eV)], \quad (1)$$

where E is the QP energy, $N(E,\varphi)$ is the QP DoS,

$$N(E,\varphi) = N(0)\mathrm{Re}\left\{\frac{E-i\Gamma(\varphi)}{\sqrt{[E-i\Gamma(\varphi)]^2-\Delta(\varphi)^2}}\right\}. \quad (2)$$

Here $\Gamma(\varphi)$ is the angular dependent QP damping factor.

Assumed angular dependencies of the gaps are shown in Fig. 3(b). In the normal state only the PG is present in antinodal parts of the barrels, $0 < \varphi < \varphi_{PG} = \pi/4 - \varphi_{Arc}/2$, with the

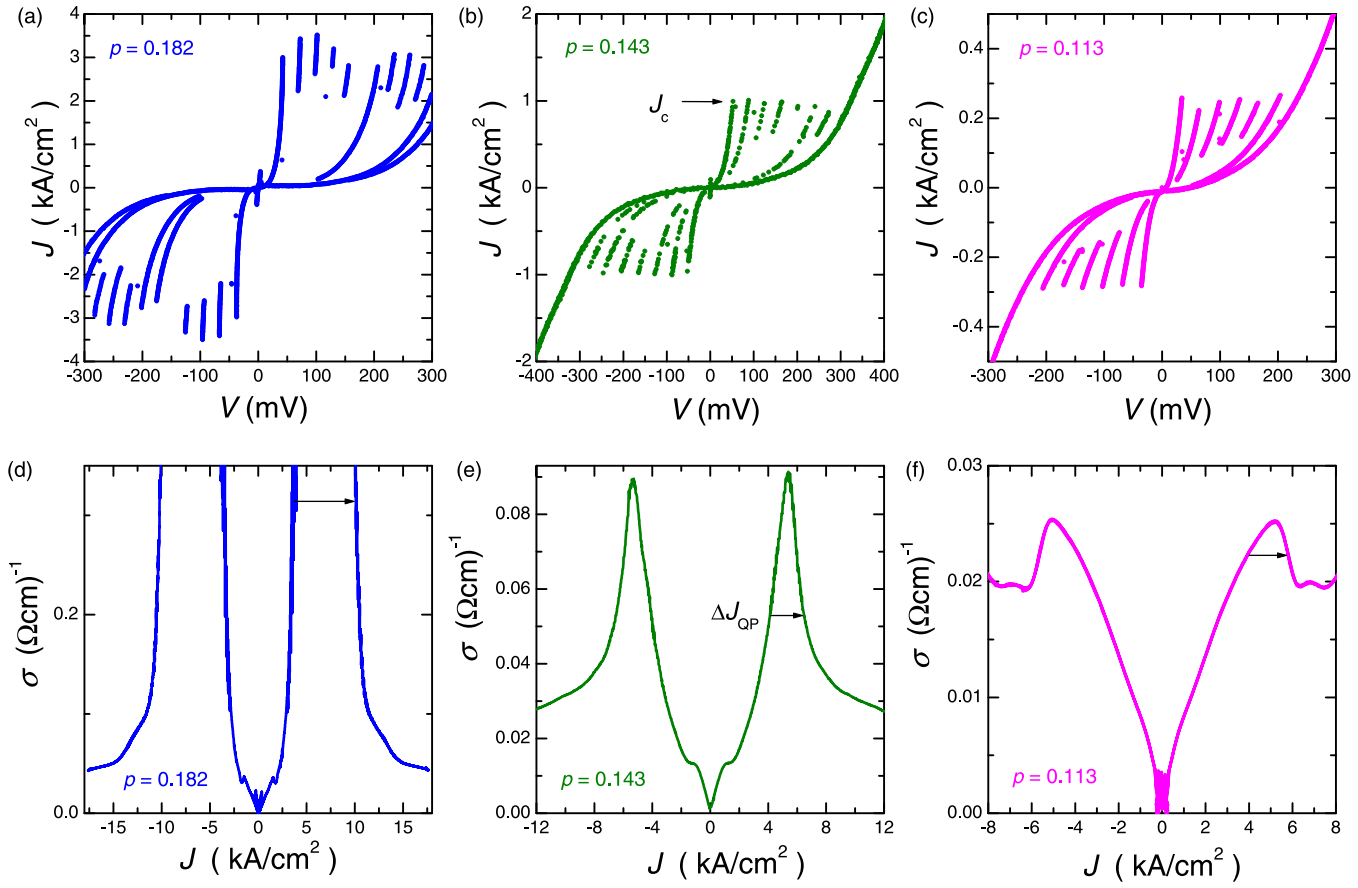

FIG. 2. (Color online) (a)–(c) Current density versus voltage characteristics for mesas with different doping. An estimation of the critical current density J_c is marked by an arrow in (b). (d)–(f) Differential conductivity versus current density characteristics for the same mesas. Arrows show estimations of the sum-gap kink amplitudes $\Delta J_{\rm QP}$.

following angular dependence:

$$\Delta_{\rm PG}(\varphi) = \Delta_{\rm PG}(0)\cos\left(\frac{\pi\varphi}{2\varphi_{\rm PG}}\right), \tag{3}$$

shown by the dashed-dotted line in Fig. 3(b). At $T < T_c$ there is a superconducting gap with a d-wave symmetry,

$$\Delta_{\rm SG}(\varphi) = \Delta_0\cos(2\varphi), \tag{4}$$

shown by the dashed line in Fig. 3(b). We assume that in the PG regions the two gaps form a combined gap

$$\Delta_{\rm Comb}(\varphi) = \sqrt{\Delta^2_{\rm PG}(\varphi) + \Delta^2_{\rm SG}(\varphi)}, \tag{5}$$

shown by the solid line in Fig. 3(b). The exact scenario in the antinodal region is not very important because the main difference between barrel and arc regions is in the QP damping $\Gamma(\varphi)$, shown in Fig. 3(c). It is large within the PG region $\Gamma_{\rm PG}(0) \sim 10$ meV [2–4], which makes QPs ill defined in the PG region, and small at the arc $\Gamma_{\rm SG} = 0.1$ meV. We assumed that the angular dependence of $\Gamma_{\rm PG}(\varphi)$ is similar to Eq. (3). Due to the large difference in Γ, the sharp sum-gap peak in dI/dV originates solely from the arc region and corresponds to the SG. In this respect the exact way in which the SG merges with the PG in the antinodal regions is not critical and Eq. (5) represents a comfortable way to connect the PG and SG regions by a continuous line.

Both the QP DoS $N(\varphi)$ and the transmission probability $\mathrm{Tr}(\varphi)$ depend on φ [45,46]. Since in Eq. (1) they appear only in a combination $\mathrm{Tr}(\varphi)N(\varphi)$, the latter represents an effective angular-dependent transmission coefficient $\mathrm{Tr}^*(\varphi)$ with respect to the case of constant DoS $N(\varphi) = N(0)$. We considered three scenarios for the angular dependence of the effective transmission coefficient $\mathrm{Tr}^*(\varphi) = \mathrm{Tr}(\varphi)N(\varphi)$.

(i) Nondirectional tunneling $\mathrm{Tr}^*(\varphi) = \mathrm{const}$, as shown by the dashed line in Fig. 3(d).

(ii) Directional tunneling with maximum in antinodal and zero transmission in nodal regions [46] $\mathrm{Tr}^*(\varphi) \propto [\cos(k_x) - \cos(k_y)]^2 \propto \{\cos[\pi\sin(\varphi)] - \cos[\pi\cos(\varphi)]\}^2$, as shown by the dashed-dotted line in Fig. 3(d). This expression is well approximated by the function $\cos(2\varphi)^2$, which we will use for analytical calculations below.

(iii) Semidirectional tunneling, which is an average of nondirectional and directional cases $\mathrm{Tr}^*(\varphi) \propto 1 + \{\cos[\pi\sin(\varphi)] - \cos[\pi\cos(\varphi)]\}^2/4$, as shown by the solid line in Fig. 3(d).

As discussed in Ref. [40], our intrinsic tunneling data are best fitted using a semidirectional $\mathrm{Tr}^*(\varphi)$ shown by the solid line in Fig. 3(d). Therefore, we present I-V calculations only for the semi-directional case. Other cases may be found in the Supplemental Material to Ref. [40]. Directional and nondirectional cases represent deviations in different directions from the best fit. They are analyzed too in

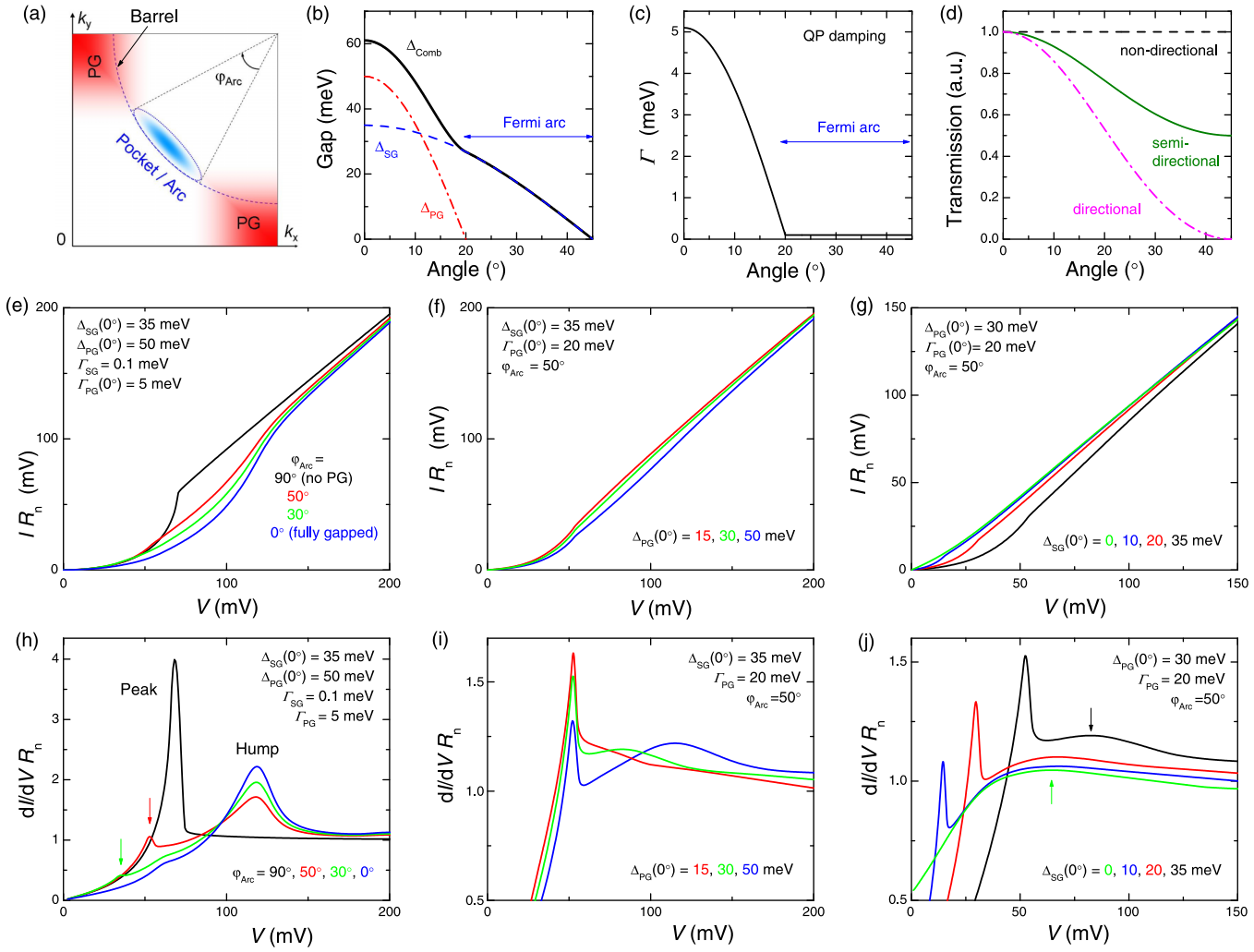

FIG. 3. (Color online) Numerical modeling of interlayer characteristics. (a) Sketch of 1/4 of the Brillouin zone. (b)–(d) Angular distribution from antinodal to nodal points of the barrel of (b) the gaps, (c) the QP damping factor, and (d) the effective transmission probability. (e)–(g) Evolution of calculated I-V curves upon varying of (e) the arc size, (f) the pseudogap energy, and (g) the superconducting gap. Note that the high-bias resistance remains unchanged because it is integrated over the same barrel. (h)–(j) Corresponding $dI/dV(V)$ curves for (e)–(g). Arrows indicate positions of peaks and humps. Calculations are made for semidirectional tunneling.

order to understand how sensitive the results are to specific parameters.

Figures 3(e)–3(g) show calculated I-Vs upon changing of (e) the arc size, (f) the PG energy, and (g) Δ_{SG}. Note that in all cases the high bias resistance remains the same. This occurs because the PG is a state-conserving gap, see Eq. (2). Therefore, the same current is recovered upon integration over the full barrel at high enough bias, irrespective whether there is a PG or not. Note that curves in Figs. 3(f) and 3(g) calculated for a large $\Gamma_{PG}(0) = 20$ meV resemble the experimental characteristics for UD mesas with a finite threshold voltage ΔV_{PG}, see Fig. 1(d).

In Fig. 3(h) we show variation of corresponding $dI/dV(V)$ curves upon changing of the arc size. $\varphi_{Arc} = 90^\circ$ corresponds to the absence of the PG. In this case the spectrum contains a single SG peak at $eV = 2\Delta_{SG}(0^\circ)$ with the shape similar to that for optimally doped and moderately UD mesas, see Figs. 1(b) and 1(d). As arcs shrink, the amplitude of the peak is rapidly decreasing and the PG hump is growing at $eV = 2\Delta_{Comb}(0^\circ)$. This is similar to evolution of experimental curves with decreasing doping, see Fig. 1(d).

Figure 3(i) demonstrates a variation of $dI/dV(V)$ upon changing the PG. When $\Delta_{PG} > \Delta_{SG}$ both the peak and the hump are present. With decreasing Δ_{PG} the hump is moving to lower V and is eventually buried under the peak. This is similar to evolution of experimental curves with increasing doping, see Figs. 1(b) and 1(d). The autonomous behavior of the SG and the PG is inherent in the considered model because the two originate from different parts of the Brillouin zone.

Figure 3(j) shows variation of $dI/dV(V)$ upon changing of Δ_{SG}, mimicking the T variation shown in Fig. 1(b). Note that the hump moves to lower V with decreasing Δ_{SG} because in our case it occurs at the combined gap $\Delta_{Comb} = \sqrt{\Delta_{PG}^2 + \Delta_{SG}^2}$. A similar shift of the hump at $T < T_c$ occurs in Fig. 1(c). We conclude that there is a good overall agreement with experimental data.

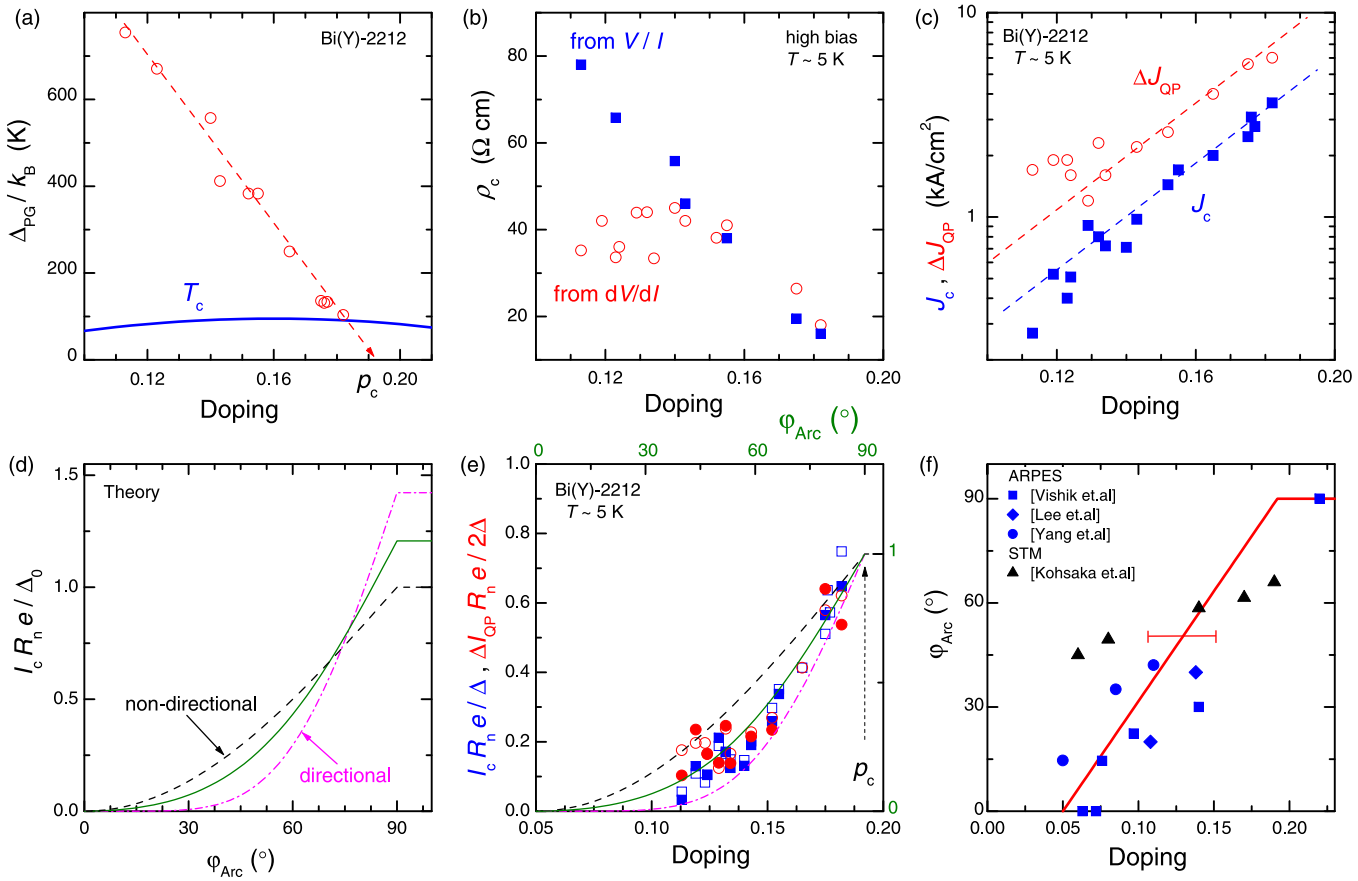

FIG. 4. (Color online) Doping dependence of (a) the pseudogap, (b) high-bias resistivities, and (c) the critical current density J_c and the sum-gap kink amplitude ΔJ_{QP}. (d) Calculated I_c from Fermi pockets, as a function of φ_{Arc} for nondirectional, semidirectional, and directional tunneling. (e) Comparison of scaled I_c and $\Delta I_{QP}/2$. They represent the amounts of Cooper pairs and QP states subjected to pairing, respectively. Lines (top-right axes) represent normalized curves from (d). The reduction of I_c and ΔI_{QP} with decreasing doping is consistent with proportional shrinkage of the Fermi pockets containing the superconducting condensate. (f) The solid line represents a deduced doping dependence of the pocket size. Symbols represent data obtained by other techniques.

IV. ANALYSIS OF DOPING DEPENDENCIES

Figure 4 represents a summary of doping dependence of intrinsic tunneling characteristics. Figure 4(a) shows the PG energy obtained from half of the PG hump voltage at $T \simeq 100$ K. It is linearly decreasing with increasing doping and tends to vanish at the critical point $p_c \simeq 0.19$ [9,18]. A topological barrel-pocket transition should occur at this point [22].

In Fig. 4(b) we analyze doping dependence of high bias resistivity. Solid and open symbols represent dc and differential (ac) values, obtained from V/I and dV/dI, respectively. For OD mesas they coincide because the I-V is Ohmic. For UD mesas the two resistances become different because the I-V is nonlinear (acquire a threshold voltage ΔV_{PG}) as a consequence of the PG, see Fig. 1(f). The linear p dependence of the dc resistivity reflects the corresponding behavior of the PG, Fig. 4(a). However, the ac resistivity becomes almost doping independent at low doping, as seen from Fig. 1(e). This requires explanation because the tunnel resistivity should carry information about the QP DoS, which changes with doping.

Simulations provide clarification of this remarkable observation. From Figs. 3(h) and 3(i) it is seen that the high-bias dI/dV is independent of φ_{Arc} and Δ_{PG}. This occurs because the PG does not change the total amount of QP states but just redistributes them. At a sufficiently high voltage $eV/N \gg \Delta_{PG}$ all QP states along the barrels, including the gapped antinodal parts, contribute to QP tunneling. The weak p dependence of ac resistivity is a consequence of the weak p dependence of barrels [3,4].

Figure 4(c) shows p dependence of J_c and ΔJ_{QP}. Both decay rapidly (almost exponentially, note the semilogarithmic scale) with decreasing doping at a rate much faster than p [10,41–43]. Thus, there is an apparent qualitative difference in doping dependencies of the Cooper pair and the high-bias QP transport. If the weak p dependence of R_n is caused by weak p dependence of barrels, then the strong $J_c(p)$ and $\Delta J_{QP}(p)$ dependencies indicate that Cooper pair current does not originate from the full length of the barrels but only from progressively shrinking with decreasing p areas, as expected for Fermi pockets.

A. Dependence of the critical current on the arc size

To find a quantitative connection between I_c and φ_{Arc} we made corresponding analytic calculations. For a junction made of s-wave superconductors $I_c R_n$ is independent of the

transmission coefficient and is given by the Ambegaokar-Baratoff expression

$$I_c R_n (T \ll T_c) = \frac{\pi \Delta}{2e}. \quad (6)$$

For coherent tunneling in a junction made of d-wave superconductors, Eq. (6) is still valid for a specific angle [48], i.e., for $\delta I_c(\varphi)\delta R_n(\varphi)$, where $\delta I_c(\varphi)$ and $\delta R_n(\varphi)$ are contributions to the critical current and resistance from Cooper pairs and QPs with momentum in the direction φ. Thus, $\delta I_c(\varphi) = \pi\Delta(\varphi)/2e\delta R_n(\varphi)$. From Eq. (1) $1/\delta R_n(\varphi) = AeN(0)^2 \mathrm{Tr}^*(\varphi)^2 \delta\varphi/2\pi$. Introducing a quantity $R_1 = AeN(0)^2$ for resistance at unit transmission $\mathrm{Tr}^* = 1$, we can write expressions for the total critical current and the normal resistance, taking into account d-wave angular dependence of the gap:

$$I_c R_1 = \frac{4}{\pi} \int_{\pi/4-\varphi_{\mathrm{Arc}}/2}^{\pi/4} \mathrm{Tr}^*(\varphi)^2 \cos(2\varphi) d\varphi, \quad (7)$$

$$R_1 R_n^{-1} = \frac{4}{\pi} \int_0^{\pi/4} \mathrm{Tr}^*(\varphi)^2 d\varphi. \quad (8)$$

Integration ranges indicate that we assumed that Cooper pair current is originating only from the arc, while QP current is accumulated over the full length of the barrel.

For the nondirectional case $\mathrm{Tr}^*(\varphi) \propto 1$ we obtain after integration of Eqs. (7) and (8):

$$I_c R_n = \frac{\Delta_0}{e}[1 - \cos(\varphi_{\mathrm{Arc}})]. \quad (9)$$

For $\varphi_{\mathrm{Arc}} = \pi/2$ it reduces to a known expression $I_c R_n = \Delta_0/e$ [48]. For the directional case, $\mathrm{Tr}^*(\varphi) \propto \cos(2\varphi)^2$,

$$I_c R_n = \frac{\Delta_0}{e}\frac{8}{3}\left[\frac{8}{15} - \cos(\varphi_{\mathrm{Arc}}) + \frac{2}{3}\cos(\varphi_{\mathrm{Arc}})^3 - \frac{1}{5}\cos(\varphi_{\mathrm{Arc}})^5\right].$$

For the semidirectional case, $\mathrm{Tr}^*(\varphi) \propto 1 + \cos(2\varphi)^2$,

$$I_c R_n = \frac{\Delta_0}{e}\frac{8}{19}\left[\frac{43}{15} - 4\cos(\varphi_{\mathrm{Arc}}) + \frac{4}{3}\cos(\varphi_{\mathrm{Arc}})^3 - \frac{1}{5}\cos(\varphi_{\mathrm{Arc}})^5\right].$$

Figure 4(d) represents the corresponding calculated dependencies $I_c R_n(\varphi_{\mathrm{Arc}})$ [49]. The solid line represents the semidirectional case, which fits best the experimental data. To check how sensitive the results are to variation of the effective transmission probability $\mathrm{Tr}^*(\varphi)$ we also considered directional and nondirectional cases, see Fig. 3(d), which correspond to deviations in two opposite directions with respect to the best fit. In all cases the I_c decreases with shrinking of the arcs and vanishes as arcs collapse $\varphi_{\mathrm{Arc}} \to 0$ because the supercurrent is originating only from arc regions. The R_n is independent of φ_{Arc} because the QP current is integrated over the whole barrel, which we assumed to be unchanged. Thus, the considered model provides a qualitative explanation of different doping dependencies of the critical current density and the high-bias differential resistance.

From Fig. 4(c) it is seen that ΔJ_{QP} and J_c are changing in a correlated manner. For d-wave tunneling $\Delta I_{\mathrm{QP}} = 2\Delta_0/eR_n = 2I_c$. In Fig. 4(e) we show correspondingly scaled quantities. They were obtained using the high bias ac resistance (open and solid symbols were obtained using different criteria for estimation of R_n and Δ). It is seen that I_c and $\Delta I_{\mathrm{QP}}/2$ indeed merge together. This confirms that both originate from the same part of the Brillouin zone, subjected to Cooper pairing. Note, however, that $J_c(p)$ decays much faster than p, i.e., suppression of the supercurrent is caused not only by reduction of the carrier density. The considered model explains well the faster than expected decay of $J_c(p)$. Lines in Fig. 4(e) represent scaled theoretical curves from Fig. 4(d). Here we assumed that $\varphi_{\mathrm{Arc}} = 90^\circ$ at the onset of the PG, $p_c \simeq 0.19$, and that $\varphi_{\mathrm{Arc}} = 0^\circ$ at the insulator-to-metal transition $p = 0.05$. The agreement between theory and experiment is remarkable taking into account that there is no fitting other than adjustment of the vertical scale.

B. Discussion

The reported qualitative difference in doping dependencies of Cooper pair (rapid decay) and high-bias quasiparticle (doping-independent) interlayer transport in Bi-2212 represents the main new experimental observation of this work, which is direct and model independent. Doping independence of the QP resistivity is intriguing and unexpected. At first glance the decrease of J_c with decreasing doping is not unexpected (provided it should follow Luttinger theorem, which is still debated) and is qualitatively consistent with observation of Uemura [50]. However, it is important to note that J_c is decreasing much faster [almost exponentially, Fig. 4(c)] than the carrier concentration p. This indicates that an additional mechanism for suppression of $J_c(p)$ is involved. Analysis of the contradictory behavior of pair and QP transport have led us to a conclusion that they originate from different parts of the Brillouin zone: pairs are residing only on small and shrinking Fermi pockets, while QP current is origination from the full length of weakly doping-dependent barrels. As seen from Fig. 4(e) this explains well the faster than expected decay of $J_c(p)$. The agreement between theory and experiment is quite remarkable.

Figure 4(f) summarizes our main result. A solid line represents the deduced Fermi pocket size as a function of doping. It is linear with p, consistent with previous reports by other techniques [16,18,19,21,22], which are also shown in the figure. It is based on the analysis of the $I_c R_n$ product from Fig. 4(e). To understand how sensitive results are to a particular angular dependence $\mathrm{Tr}^*(\varphi)$, we considered directional and nondirectional cases with deviations of $\mathrm{Tr}^*(\varphi)$ in two opposite directions with respect to the best fit (semidirectional case), see Fig. 3(d). From Fig. 4(e) it is seen that estimation of φ_{Arc} is affected only marginally by a particular $\mathrm{Tr}^*(\varphi)$ because calculated curves for the optimal (semidirectional) and the two extreme (directional and nondirectional) cases all lay within the data spread. Thus, our quantitative conclusions in Fig. 4(f) are not sensitive to specific parameters of the model. The corresponding uncertainty is indicated by the horizontal error bar in Fig. 4(f).

Our qualitative conclusions are robust because they are based entirely on directly measured experimental data. Calculated dI/dV curves are presented to show an autonomous

behavior of the SG peak and the PG hump in the considered model. All additional factors (singularities in DoS due to competing orders or band structure, nontrivial angular dependence of characteristics, etc.) would affect the shape but would not change the autonomous behavior of the peak and the hump, which is inherent for this model because SG and PG are originating from different parts of the Brillouin zone.

To conclude, an important new aspect of our work lies in the unique ability of intrinsic Josephson junctions to independently probe Cooper pair and quasiparticle transport. Our main result is observation of rapid (much faster than p) decay of the pair current with decreasing doping and almost p-independent quasiparticle resistance. This indicates that the QP current is originating from the full area of large, weakly doping-dependent barrels. However, the Cooper pair current originates only from small Fermi pockets, which shrink with decreasing doping. The antinodal parts of barrels, which grow bigger with underdoping, do not contribute to supercurrent. This provides a direct evidence for nonsuperconducting origin of the pseudogap in cuprates.

ACKNOWLEDGMENTS

The work was supported by the Swedish Research Council Grant No. 621-2014-4314, the Swedish Foundation for International Cooperation in Research and Higher Education Grant No. IG2013-5453 and the Swiss National Science Foundation grant Sinergia No. CRSII2-154410/1. Technical support from the Core Facility in Nanotechnology at Stockholm University is gratefully acknowledged.

[1] W. E. Pickett, H. Krakauer, R. E. Cohen, and D. J. Singh, Science **255**, 46 (1992).
[2] A. Damascelli, Z. Hussain, and Z.-X. Shen, Rev. Mod. Phys. **75**, 473 (2003).
[3] A. A. Kordyuk, S. V. Borisenko, M. S. Golden, S. Legner, K. A. Nenkov, M. Knupfer, J. Fink, H. Berger, L. Forro, and R. Follath, Phys. Rev. B **66**, 014502 (2002).
[4] F. Ronning, T. Sasagawa, Y. Kohsaka, K. M. Shen, A. Damascelli, C. Kim, T. Yoshida, N. P. Armitage, D. H. Lu, D. L. Feng, L. L. Miller, H. Takagi, and Z.-X. Shen, Phys. Rev. B **67**, 165101 (2003).
[5] K. B. Dave, P. W. Phillips, and C. L. Kane, Phys. Rev. Lett. **110**, 090403 (2013).
[6] A. Kanigel, M. R. Norman, M. Randeria, U. Chatterjee, S. Souma, A. Kaminski, H. M. Fretwell, S. Rosenkranz, M. Shi, T. Sato, T. Takahashi, Z. Z. Li, H. Raffy, K. Kadowaki, D. Hinks, L. Ozyuzer, and J. C. Campuzano, Nat. Phys. **2**, 447 (2006).
[7] T. Timusk and B. Statt, Rep. Prog. Phys. **62**, 61 (1999).
[8] V. M. Krasnov, A. Yurgens, D. Winkler, P. Delsing, and T. Claeson, Phys. Rev. Lett. **84**, 5860 (2000).
[9] J. L. Tallon and J. W. Loram, Physica C **349**, 53 (2001).
[10] V. M. Krasnov, Phys. Rev. B **65**, 140504(R) (2002).
[11] D. van der Marel, H. J. A. Molegraaf, J. Zaanen, Z. Nussinov, F. Carbone, A. Damascelli, H. Eisaki, M. Greven, P. H. Kes, and M. Li, Nature (London) **425**, 271 (2003).
[12] M. R. Norman, D. Pines, and C. Kallin, Adv. Phys. **54**, 715 (2005).
[13] H.-B. Yang, J. D. Rameau, P. D. Johnson, T. Valla, A. Tsvelik, and G. D. Gu, Nature (London) **456**, 77 (2008).
[14] A. D. LaForge, W. J. Padilla, K. S. Burch, Z. Q. Li, A. A. Schafgans, K. Segawa, Y. Ando, and D. N. Basov, Phys. Rev. Lett. **101**, 097008 (2008).
[15] A. Pushp, C. V. Parker, A. N. Pasupathy, K. K. Gomes, S. Ono, J. Wen, Z. Xu, G. Gu, and A. Yazdani, Science **324**, 1689 (2009).
[16] W. S. Lee, I. M. Vishik, K. Tanaka, D. H. Lu, T. Sasagawa, N. Nagaosa, T. P. Devereaux, Z. Hussain, and Z.-X. Shen, Nature (London) **450**, 81 (2007).
[17] S.-I. Ideta, T. Yoshida, A. Fujimori, H. Anzai, T. Fujita, A. Ino, M. Arita, H. Namatame, M. Taniguchi, Z.-X. Shen, K. Takashima, K. Kojima, and S.-I. Uchida, Phys. Rev. B **85**, 104515 (2012).
[18] I. M. Vishik, M. Hashimoto, R.-H. He, W.-S. Lee, F. Schmitt, D. Lu, R. G. Moore, C. Zhang, W. Meevasana, T. Sasagawa, S. Uchida, K. Fujita, S. Ishida, M. Ishikado, Y. Yoshida, H. Eisaki, Z. Hussain, T. P. Devereaux, and Z.-X. Shen, Proc. Natl. Acad. Sci. USA **109**, 18332 (2012).
[19] Y. Kohsaka, C. Taylor, P. Wahl, A. Schmidt, J. Lee, K. Fujita, J. W. Alldredge, K. McElroy, J. Lee, H. Eisaki, S. Uchida, D.-H. Lee, and J. C. Davis, Nature (London) **454**, 1072 (2008).
[20] J. Meng, G. Liu, W. Zhang, L. Zhao, H. Liu, X. Jia, D. Mu, S. Liu, X. Dong, J. Zhang, W. Lu, G. Wang, Y. Zhou, Y. Zhu, X. Wang, Z. Xu, C. Chen, and X. J. Zhou, Nature (London) **462**, 335 (2009).
[21] H.-B. Yang, J. D. Rameau, Z.-H. Pan, G. D. Gu, P. D. Johnson, H. Claus, D. G. Hinks, and T. E. Kidd, Phys. Rev. Lett. **107**, 047003 (2011).
[22] B. Vignolle, D. Vignolles, D. LeBoeuf, S. Lepault, B. Ramshaw, R. Liang, D. A. Bonn, W. N. Hardy, N. Doiron-Leyraud, A. Carrington, N. E. Hussey, L. Taillefer, and Cyril Proust, C. R. Phys. **12**, 446 (2011).
[23] E. A. Yelland, J. Singleton, C. H. Mielke, N. Harrison, F. F. Balakirev, B. Dabrowski, and J. R. Cooper, Phys. Rev. Lett. **100**, 047003 (2008).
[24] M. V. Kartsovnik, T. Helm, C. Putzke, F. Wolff-Fabris, I. Sheikin, S. Lepault, C. Proust, D. Vignolles, N. Bittner, W. Biberacher, A. Erb, J. Wosnitza, and R. Gross, New J. Phys. **13**, 015001 (2011).
[25] S. C. Riggs, O. Vafek, J. B. Kemper, J. B. Betts, A. Migliori, F. F. Balakirev, W. N. Hardy, R. Liang, D. A. Bonn, and G. S. Boebinger, Nat. Phys. **7**, 332 (2011).
[26] N. Barisic, S. Badoux, M. K. Chan, C. Dorow, W. Tabis, B. Vignolle, G. Yu, J. Beard, X. Zhao, C. Proust, and M. Greven, Nat. Phys. **9**, 761 (2013).
[27] S. E. Sebastian, N. Harrison, F. F. Balakirev, M. M. Altarawneh, P. A. Goddard, R. Liang, D. A. Bonn, W. N. Hardy, and G. G. Lonzarich, Nature (London) **511**, 61 (2014).
[28] S. Chakravarty, Rep. Prog. Phys. **74**, 022501 (2011).
[29] V. J. Emery and S. A. Kivelson, Nature (London) **374**, 434 (1995).
[30] V. M. Krasnov, Phys. Rev. B **79**, 214510 (2009).
[31] V. M. Krasnov, H. Motzkau, T. Golod, A. Rydh, S. O. Katterwe, and A. B. Kulakov, Phys. Rev. B **84**, 054516 (2011).
[32] Th. Jacobs, S. O. Katterwe, H. Motzkau, A. Rydh, A. Maljuk, T. Helm, C. Putzke, E. Kampert, M. V. Kartsovnik, and V. M. Krasnov, Phys. Rev. B **86**, 214506 (2012).

[33] E. Gull, O. Parcollet, and A. J. Millis, Phys. Rev. Lett. **110**, 216405 (2013).
[34] T. Ekino, A. M. Gabovich, M. S. Li, M. Pekala, H. Szymczak, and A. I. Voitenko, J. Phys.: Condens. Matter **20**, 425218 (2008).
[35] A. Dubroka, M. Rössle, K. W. Kim, V. K. Malik, D. Munzar, D. N. Basov, A. A. Schafgans, S. J. Moon, C. T. Lin, D. Haug, V. Hinkov, B. Keimer, Th. Wolf, J. G. Storey, J. L. Tallon, and C. Bernhard, Phys. Rev. Lett. **106**, 047006 (2011).
[36] T. Kondo, Y. Hamaya, A. D. Palczewski, T. Takeuchi, J. S. Wen, Z. J. Xu, G. Gu, J. Schmalian, and A. Kaminski, Nat. Phys. **7**, 21 (2011).
[37] R. Kleiner and P. Müller, Phys. Rev. B **49**, 1327 (1994).
[38] S. O. Katterwe, A. Rydh, H. Motzkau, A. B. Kulakov, and V. M. Krasnov, Phys. Rev. B **82**, 024517 (2010).
[39] A. Barone and C. Paterno, *Physics and Applications of the Josephson Effect* (John Wiley and Sons, New York, 1982).
[40] S. O. Katterwe, A. Rydh, and V. M. Krasnov, Phys. Rev. Lett. **101**, 087003 (2008).
[41] A. Irie and G.-I. Oya, Physica C **367**, 393 (2002).
[42] K. Inomata, T. Kawae, K. Nakajima, S.-J. Kim, and T. Yamashita, Appl. Phys. Lett. **82**, 769 (2003).
[43] H. Kambara, I. Kakeya, and M. Suzuki, Phys. Rev. B **87**, 214521 (2013).
[44] J. K. Ren, X. B. Zhu, H. F. Yu, Y. Tian, H. F. Yang, C. Z. Gu, N. L. Wang, Y. F. Ren, and S. P. Zhao, Sci. Rep. **2**, 248 (2012).
[45] M. R. Norman, M. Randeria, H. Ding, and J. C. Campuzano, Phys. Rev. B **52**, 615 (1995).
[46] L. B. Ioffe and A. J. Millis, Phys. Rev. B **58**, 11631 (1998).
[47] Y. Yamada and M. Suzuki, Phys. Rev. B **66**, 132507 (2002).
[48] Y. Tanaka and S. Kashiwaya, Phys. Rev. B **56**, 892 (1997).
[49] Calculations of $I_c R_n$ are made only along the arc, which as we assume, represent one side of the Fermi pocket. The other side of the pocket will provide a similar contribution to I_c. This may change the numerical coefficient in front of those equations, but will not significantly change the functional dependence $I_c R_n(\varphi_{\mathrm{Arc}})$. Since estimation of φ_{Arc} is made only from the shape of the $I_c R_n(\varphi_{\mathrm{Arc}})$ dependence, see Fig. 4(e), the change in the prefactor will not affect our results.
[50] Y. J. Uemura, J. Phys.: Condens. Matter **16**, S4515 (2004).